Int. J. Heat Mass Transfer. Vol. 25, No. 4, pp. 541–552, 1982
Printed in Great Britain

0017–9310/82/040541–12 $03.00/0

FORCED FLOW EVAPORATIVE COOLING OF A VOLUMETRICALLY HEATED POROUS LAYER*

A. S. NAIK and V. K. DHIR
Chemical, Nuclear and Thermal Engineering Department,
University of California, Los Angeles, U.S.A.

(*Received* 27 *May* 1981 *and in revised form* 29 *September* 1981)

Abstract—In this paper, the temperature rise and pressure drop experienced by an evaporating coolant flowing through a volumetrically heated porous layer have been studied experimentally. Experimental data for the temperature distribution and the two-phase pressure drop along the direction of flow is obtained for water flowing through layers of inductively heated steel particles. Spherical steel particles varying in size from 590 to 4763 μm are used to form porous layers in 5 and 10 cm dia. glass jars. In these experiments the data are obtained for layer depths varying from 9 to 81 cm, volumetric heat generation rate varying from 1.44 to 44.0 W/cm^3 and the mass flow rate of water varying from 510 to 18200 kg/m^2 h.

A theoretical model for the temperature profile in the liquid region and the two phase region has been made and is found to compare well with the measurements. Vapor channels are observed to form in porous layers of particle diameter less than 1600 μm. Separate semi-theoretical models have been developed for the two phase pressure drop in particles with diameter less than and greater than 1600 μm.

NOMENCLATURE

A, $= \pi D^2/4$, area of cross-section of the porous layer [cm^2];
a, viscous coefficient in the Kozeny–Carman equation [cm^{-2}];
b, inertial coefficient in the Kozeny–Carman equation [cm^{-1}];
c_0, empirical constant;
$c_{pv}, c_{pl}, c_{pf}, c_{pp}$, specific heat at constant pressure of vapor, liquid, fluid, and particles, respectively [kcal/kg K];
c_{pm}, $= c_{pf}\varepsilon + c_{pp}(1-\varepsilon)$, specific heat of mixture (fluid and particles) at constant pressure [kcal/kg K];
D, inner diameter of the glass jar [cm];
d_c, diameter of the vapor channels [mm];
d_p, diameter of particle [cm];
f, local friction factor through vapor channel;
$\bar{f}$, average friction factor through the vapor channel;
G_f, mass velocity of liquid at inlet or of the two phase mixture [kg/m^2 s];
g, acceleration of gravity [m/s^2];
H, depth of the particulate bed [cm];
h_{fg}, latent heat of vaporization [kcal/kg];
h_v, volumetric particle to fluid heat transfer coefficient [W/m^3 K];
k_f, k_p, thermal conductivity of fluid (vapor or liquid) and particles, respectively [W/m K];
k_m, $= \varepsilon k_f + (1-\varepsilon)k_p$, mean thermal conductivity of the mixture (fluid and particles) [W/m K];
l, $= b/a$, ratio of the inertial and viscous coefficients in the Kozeny–Carman equation [cm];
m_l, mass of liquid in the porous layer [kg];
m_p, mass of particles in the porous layer [kg];
$\dot{m}_v, \dot{m}_l$, mass flow rate of vapor and liquid respectively [kg/s];
$\dot{m}_{le}$, mass flow rate of liquid at exit;
N, number of vapor channels per unit area of cross-section [number/cm^2];
P, pressure [N/m^2];
ΔP_f, frictional pressure drop in the two phase region [N/m^2];
ΔP_0, hydrostatic head in the two phase region if it was filled with saturated liquid [N/m^2];
ΔP_t, total pressure drop in the two phase region [N/m^2];
$\dot{Q}_v, \bar{\dot{Q}}_v$, local and average volumetric heat generation rates in the porous bed [W/cm^3];
$\dot{Q}_T$, total power generated in the porous bed [W];
T_f, T_p, T_m, temperature of the fluid, particles and mixture, respectively [°C];
T_{fi}, inlet temperature of liquid [°C];
T_{sat}, saturation temperature of the liquid [°C];
v_v, v_l, specific volume of vapor and liquid respectively [m^3/kg];
x, quality of the two phase mixture $[\dot{m}_v/\dot{m}]$;
x_e, quality of the mixture at the exit of the porous bed;

*The paper was presented at the 20th ASME/AIChE National Heat Transfer Conference, Milwaukee, Wisconsin, 2–5 Aug. 1981.

z, axial distance along the direction of flow [cm];
z_l, axial distance at which liquid just begins to evaporate [cm];
z_k, axial distance at which vapor just begins superheating [cm];

Greek symbols

α, fractional cross-section area occupied by vapor in the two phase region;
ε, the porosity of the porous layer;
η, the mass fraction of total vapor flow rate flowing through the non-channeled region;
μ_v, μ_l, the viscosity of vapor and liquid, respectively [kg/m s];
ν_v, ν_l, the kinematic viscosity of vapor and liquid, respectively [m^2/s];
ρ_v, ρ_l, ρ_p, the density of vapor, liquid and particles, respectively [kg/m^3].

Subscripts

c, channel;
f, fluid;
l, liquid;
m, mixture;
nc, non-channeled region;
p, particle.

Superscript

average over z.

INTRODUCTION

AFTER a hypothetical transient overpower accident or a transient undercooling accident in a liquid metal fast breeder reactor, fuel debris may collect in the coolant channels in the form of a porous blockage. The recent incident at the Three Mile Island-2 nuclear power plant has also shown that during severe undercooling conditions, the fuel elements of a light water reactor may deform to such an extent that certain portions of the core may behave as a heat generating porous blockage. Several analytical and experimental studies exist in the literature that attempt to understand the heat transfer characteristics of single phase flow through a volumetrically heated porous plug. However, few experimental or theoretical studies have been made to understand the complex thermal–hydraulic characteristics of a porous layer when two phase flow conditions exist in the plug. In the present work, thermal–hydraulic characteristics of a volumetrically heated porous layer subjected to forced flow boiling are studied experimentally.

The earliest theoretical and experimental study of the thermal–hydraulic characteristics of single phase flow through a volumetrically heated porous layer is that of Choudhary and El-Wakil [1]. They solved the coupled linear energy equations for the solid and the gas phase using an implicit modified Crank–Nicholson method. The pressure drop through the porous layer was determined by using the Kozeny–Carman equation with both viscous and inertia terms in it. By comparing the measured exit fluid temperature history with solutions of the energy equations, they correlated volumetric heat transfer coefficient data by

$$Nu_l = (Re_l)^{0.65}\left[\frac{l(1-\varepsilon)}{0.00377}\right]^{1.33} \quad (1)$$

In equation (1), l, is the characteristic length defined as the ratio of inertial and viscous coefficients in the Kozeny–Carman equations for pressure drop, while Re_l and Nu_l are defined as

$$Re_l = \frac{lG_f}{\mu_f}, \quad (2)$$

$$Nu_l = \frac{h_v l^2}{k_f}. \quad (3)$$

The numerical constant, 0.00377, in equation (1) was measured in feet.

The steady state analysis of [1] has been extended to single phase transient cooling of a volumetrically heated porous layer [2].

Motivated by its potential application to nuclear power thermal reactors, Moalem and Cohen [3–5], analyzed fluid flow through a volumetrically heated porous layer under phase change and vapor superheat conditions. The temperature distributions in the solid and fluid phases were obtained by simultaneously solving the energy equation for each phase. The pressure drop through the porous layer was obtained by using the Kozeny–Carman relation. Characteristic parameters for various operational conditions of the reactor were evaluated. In their work Moalem and Cohen gave no particular attention to the pressure drop in the two phase region lying between the single phase liquid and superheated vapor regions.

Vasiliev and Mairov [6] have analyzed heat transfer, pressure drop and stability characteristics of a volumetrically heated porous layer cooled with forced flow evaporation. Dependent upon the physical state of the coolant, they divided the porous layer into three regions—subcooled, saturated two phase mixture and superheated steam. For each region, they solved the energy equations with appropriate boundary and interfacial conditions to obtain temperature distribution in the solid and the fluid. The energy equations used in [6] are similar to those used in the present work and as such are not reproduced here. The pressure drop through different regions was calculated by using Kozeny–Carman equation:

$$-\frac{dP}{dz} = avG_f + bvG_f^2 \quad (4)$$

where

$$a \equiv \frac{150(1-\varepsilon)^2}{\varepsilon^3 d_p^2}, \quad b \equiv \frac{1.75(1-\varepsilon)}{\varepsilon^3 d_p}.$$

To use equation (4) in the two phase region, they defined the specific volume of the mixture as

$$v = v_l + x(v_v - v_l) \tag{5}$$

while two alternative formulations were used to define the kinematic viscosity of the mixture

$$\nu_I = \nu_l + x(\nu_v - \nu_l) \tag{6}$$

and

$$\nu_{II} = [\mu_l + x(\mu_v - \mu_l)]\,[v_l + x(v_v - v_l)]. \tag{7}$$

Hydrodynamic and thermal characteristics of the evaporative cooling of the porous layer allowed them to analyze the stability of the process.

The modeling of the two phase pressure drop in the work of [6] is speculative and does not have a sound physical basis. Also, the orientation of flow in the studies of [5, 6] is normal to the gravitational acceleration whereas in physical situations of interest in light water and liquid metal fast breeder reactor safety, the gravity acts in a direction parallel to the flow.

The purpose of this work is to obtain data for the steady state temperature profile and pressure drop of an evaporating coolant flowing vertically through an inductively heated porous layer. Data will be taken for various particle sizes, layer depths, volumetric heat generation rates and mass flow rates of water. The observed temperature profiles and the two phase pressure drop will be compared with those predicted by the theoretical and semi-theoretical models developed in this work and elsewhere. At present no such data or comparison of the data with the theoretical models exist in the literature.

ANALYSIS

Preliminary visual observations indicated the formation of vapor channels in small diameter particles ($d_p \leq 1600\,\mu$m). In large diameter particles ($1600 < d_p < 4763\,\mu$m) the vapor appeared to flow in the interstitial spaces between the particles. This suggested that probably two models were needed to describe the two phase pressure drop in small and large diameter particles. However, a single model could be used to determine temperature distribution in the particulate layers as long as the Biot number based on the particle radius was less than unity.

Temperature distribution

The steady state 1-dim. energy equations describing the temperature of the particles and the coolant can be written as

$$k_p(1-\varepsilon)\frac{d^2T_p}{dz^2} - h_v(T_p - T_f) + \dot{Q}_v(z) = 0, \tag{8}$$

$$k_f\varepsilon\frac{d^2T_f}{dz^2} + h_v(T_p - T_f) - G_f c_{pf}\frac{dT_f}{dz} = 0. \tag{9}$$

The coordinate system utilized in writing equations (8) and (9) is shown in Fig. 1. In the single phase liquid region, the volumetric heat transfer coefficient given by equation (1) for water is sufficiently large so that the difference between the particle and liquid temperature can be safely assumed to be small. Defining a mean temperature, T_m, as

$$T_m = T_p = T_f \tag{10}$$

and a mean thermal conductivity, k_m, as

$$k_m = k_p(1-\varepsilon) + k_f\varepsilon. \tag{11}$$

Equations (8) and (9) can be added to give:

$$k_m\frac{d^2T_m}{dz^2} - G_f c_{pf}\frac{dT_m}{dz} + \dot{Q}_v(z) = 0. \tag{12}$$

The boundary conditions for equation (12) are the conductive heat loss from the bottom of porous layer that produces a jump in the liquid temperature:

$$k_m\frac{dT_m}{dz} = G_f c_{pf}(T_m - T_{fi}) \text{ at } z = 0, \tag{13}$$

and the zero heat flux condition at the height, z_l, where liquid reaches its saturation temperature:

$$\frac{dT_m}{dz} = 0 \quad \text{at} \quad z = z_l \tag{14}$$

The height, z_l, where boiling begins is obtained by

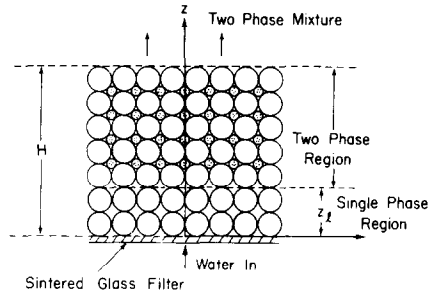

a) Vapor Flow Model For Large Particles (d_p > 1600 μm)

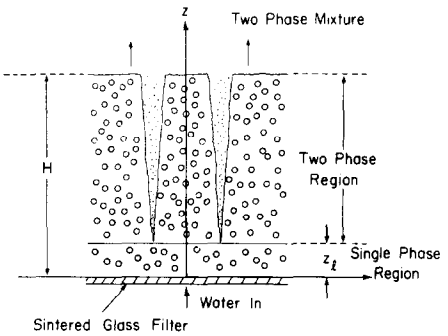

b) Vapor Flow Model For Small Particles (d_p < 1600 μm)

FIG. 1. Models for two phase pressure drop in large and small diameter particles.

making an energy balance as

$$\int_0^{z_1} \dot{Q}_v(z)\,dz = G_f c_{pf}(T_{sat} - T_{fi}). \quad (15)$$

Assuming that $\dot{Q}_v(z) = A + Bz$ represents the variation of $\dot{Q}_v$ with z in the liquid region, the solution of equation (12) consisting of both homogeneous and particular parts is obtained as

$$T_m = c_1 + c_2 \exp(G_f c_{pf} z/k_m) + cz + Dz^2 \quad (16)$$

where

$$D = B/2G_f c_{pf}, \quad (17)$$

$$c = \left(A + \frac{k_m B}{G_f c_{pf}}\right)\Big/(G_f c_{pf}), \quad (18)$$

$$c_1 = T_{fi} + (k_m c/G_f c_{pf}), \quad (19)$$

$$c_2 = -(c + 2Dz_1)\frac{k_m}{G_f c_{pf}}\exp(-G_f c_{pf} z_1/k_m). \quad (20)$$

The solution equation (16) could easily be extended to the cases where the volumetric heat generation is represented by a polynomial of the nth degree.

After the liquid reaches its saturation temperature, the energy generated in the particles will be utilized to convert the liquid into vapor. In the two phase region, the volumetric heat transfer coefficient, h_v, is expected to be large. Thus, the temperature difference between the particles and the fluid will be small. If the pressure drop through the porous layer is much smaller than the system pressure, the variation of T_{sat} in the two phase region due to variation in pressure can be neglected and it can be assumed that

$$T_f = T_{sat} \quad (21)$$

until all the liquid is converted into vapor. In the two phase region the quality, x, at any location z is determined from the energy balance equation as

$$x = \left[\int_0^z \dot{Q}_v(z)\,dz - G_f c_{pf}(T_{sat} - T_{fi})\right]\Big/ G_f h_{fg}. \quad (22)$$

After the quality attains a value equal to unity, the vapor can be superheated. The location, z_k, at which vapor starts to superheat is obtained from equation (22) when x is taken to be 1.

Pressure drop

In the non-boiling region, the single phase pressure drop irrespective of the particle size can be calculated by using the Kozeny–Carman equation (4). Moreover for two phase pressure drop different models are needed depending upon whether vapor channels are formed in the particulate layer or not.

Homogeneous model for pressure drop in large diameter particles ($d_p > 1600\,\mu m$). Figure 1a shows a conceptual configuration of two phase flow through large diameter spherical particles. Vapor and liquid phases move through the interstitial spaces between the particles. Assuming that the average fractional cross-sectional area of the particulate layer occupied by vapor is α, the pressure drop experienced by liquid and vapor phases in moving a distance, dz, in the vertical direction can be written:

$$-(dp_v)\alpha = F_{Dv}/A + F_{Di}/A + \rho_v g\alpha dz \quad (23)$$

$$-(dp_l)(1-\alpha) = F_{Dl}/A + F_{Di}/A + \rho_l g(1-\alpha)\,dz. \quad (24)$$

In equations (23) and (24), F_{Dv} and F_{Dl} are the particle drag forces on vapor and liquid phases respectively and F_{Di} is the drag at the vapor liquid interface. The change in momentum as a result of increase in specific volume after evaporation has been neglected in these two equations. For the low mass flow rates studied in this work, the interfacial drag can be neglected in comparison to the particle drag. Combining equations (23) and (24), the two phase pressure drop across the differential element dz is obtained as

$$-dp_t = -(dp_v)\alpha - (dp_l)(1-\alpha)$$
$$= F_{Dv}/A + F_{Dl}/A + (\rho_v g\alpha + \rho_l g(1-\alpha))\,dz. \quad (25)$$

The first two terms on the extreme right-hand side of equation (25) represent the friction pressure drop whereas the last term represents the hydrostatic head. Using equation (4), the drag forces F_{Dv} and F_{Dl} are written as

$$F_{Dv} = (av_v x G_f/\alpha + bx^2 G_f^2/\rho_v\alpha^2)A\,dz, \quad (26)$$

$$F_{Dl} = [av_l(1-x)G_f/(1-\alpha) + b(1-x)^2 G_f^2/\rho_l(1-\alpha)^2]A\,dz \quad (27)$$

In equations (26) and (27), the quality, x, at any location z is obtained from equation (22). Substituting for F_{Dv} and F_{Dl} from equations (26) and (27) into (25) and dividing throughout by dz, an expression for total pressure gradient in the direction of flow is obtained:

$$-\frac{dp_t}{dz} = a\left(\frac{v_v x}{\alpha} + \frac{v_l(1-x)}{(1-\alpha)}\right)G_f + b\left(\frac{x^2}{\rho_v\alpha^2} + \frac{(1-x)^2}{\rho_l(1-\alpha)^2}\right)G_f^2 + \rho_v g\alpha + \rho_l g(1-\alpha). \quad (28)$$

The two phase pressure drop in the porous layer can be calculated from equation (28) once a relation between x and α is known. Many investigations in the literature have attempted to determine α, by minimizing with respect to α, the presssure drop given by equation (28). However this is purely speculative and no rationale can be advanced for such an assumption. Comparison of the coefficients of G_f and G_f^2 in equation (28) with Vasiliev and Mairov's equations (5)–(7) shows that effective viscosity and specific volume of the two phase flow given by equation (28) are much different. In the present work an empirical relation between x and α will be obtained by comparing the two phase pressure drop given by equation (28) with the observed pressure drop.

Channel flow model for pressure drop in small diameter particles ($d_p < 1600\,\mu m$). Figure 1b shows the vapor flow configuration in porous layers composed of small diameter particles. In these layers the vapor bubbles are able to push the particles away and thus escape in the form of channels or tunnels located discretely in the porous layer. The channels are free of any particles. Since all of the vapor is generated in the non-channeled region, vapor bubbles will flow a certain distance in the non-channeled region before merging into the vapor channels. Assuming that all of the liquid flows through the non-channeled region, the total pressure drop based on the homogeneous model in the non-channeled region can be written in a manner similar to equation (28) as

$$\frac{(dp_t)_{nc}}{dz} = a\left(\frac{v_v x\eta}{\alpha} + \frac{v_l(1-x)}{(1-\alpha)}\right)G_f + b\left(\frac{x^2\eta^2}{\rho_v\alpha^2} + \frac{(1-x)^2}{\rho_l(1-\alpha)^2}\right)G_f^2 + \alpha\rho_v g + \rho_l(1-\alpha)g. \tag{29}$$

Using a formulation similar to that for flow in pipes, the pressure drop in the channeled portion can be written as

$$\frac{(dp_t)_c}{dz} = \frac{8f(1-\eta)^2x^2G_f^2}{\pi^2 d_c^5\rho_v N^2} + \rho_v g. \tag{30}$$

In equation (30) f is the friction factor, N is the number of channels per unit cross-sectional area of the porous layer and d_c is the local diameter of the channel. The friction factor, f, is defined as

$$f = \frac{c_0}{Re^n} \equiv \frac{c_0}{[4G_f(1-\eta)x/\pi N\mu_v d_c)^n} \tag{31}$$

Equations (29)–(31) give us only three equations in eight unknowns $(dp_t)_{nc}/dz$, $(dp_t)_c/dz$, η, d_c, N, f, c_0 and n. To solve explicitly for all the unknowns five more relations are needed. These relations can be obtained by making some assumptions or using experimental information. In this work it is proposed that:

(i) the pressure gradient in the non-channeled and channeled region is the same

$$\frac{(dp_t)_{nc}}{dz} = \frac{(dp_t)_c}{dz} \tag{32}$$

In equation (32), pressure difference due to surface tension between vapor channel and the surrounding region has been neglected because a well defined liquid–vapor–solid interface does not exist.

(ii) The flow in the vapor channels is laminar so that the friction factor varies inversely with Reynolds number. Or in equation (30), the exponent

$$n = 1 \tag{33}$$

This assumption will be true over a limited range of mass flow velocity, G_f, and its validity for the present set of data will be checked.

(iii) The total two phase pressure drop across the porous layer is obtained by integrating either equation (29) or (30) and is known from experiments

$$\Delta P_t = (\Delta P_t)_{nc} = (\Delta P_t)_c = -\int_{z_i}^{H}\frac{(dp_t)_c}{dz}dz. \tag{34}$$

(iv) The vapor channels begin to form at a location where boiling begins. The average vapor channel diameter (d_{ce}) at exit (top of the porous layer) and number of vapor channels, N per unit area, are also known from experiments. The vapor channel diameter at any location is proportional to local quality, i.e.

$$\frac{d_c}{d_{ce}} = \frac{x}{x_e}. \tag{35}$$

Evidently vapor channel of zero diameter has no physical meaning. Thus the vapor channel diameter where boiling begins ($x = 0$) is taken to be equal to the diameter of the largest circle that can be drawn in the interstitial space between three adjoining particles placed at the corners of an equilateral triangle [7].

For a given flow rate and heat generation rate, the numerical procedure consists of solving equations (12), (29)–(32) simultaneously along the direction of flow with assumed value of c_0 and with *a priori* knowledge of d_{ce} and N. Functional dependence of α_{nc} upon local quality is obtained from pressure drop model for large diameter particles. Thereafter equation (34) is integrated. The calculated total pressure drop across the boiling region is compared with the observed pressure drop and a new value of c_0 is obtained. The procedure is repeated until the guessed value of c_0 is the same as that obtained by solving equation (34).

EXPERIMENTAL MEASUREMENTS

The experimental apparatus was designed so that temperature distribution and pressure drop across a volumetrically heated porous layer cooled by a vertically upward flowing liquid undergoing phase change could be studied. Distilled water was used as the coolant while a packed column of inductively heated steel particles was used to simulate a volumetrically heated porous layer. The particle size, height of the porous layer, heat generation rate and the exit quality were varied parametrically.

Apparatus and procedure

The main components of the experiment set up are: a glass jar filled with steel particles, an induction heater, a work coil, a water reservoir and a centrifugal pump. The instrumentation consists of thermocouples with an X–Y recorder for measuring temperatures and a manometer or capsuhelic gauge for measuring the pressure drop. A schematic diagram of the apparatus is shown is Fig. 2. The quartz jar used for forming the porous layer has an i.d. of 102 mm and is 348 mm high. A sintered glass filter 6 mm in thickness and having a permeability of 170–220 μm is welded at 30 mm from

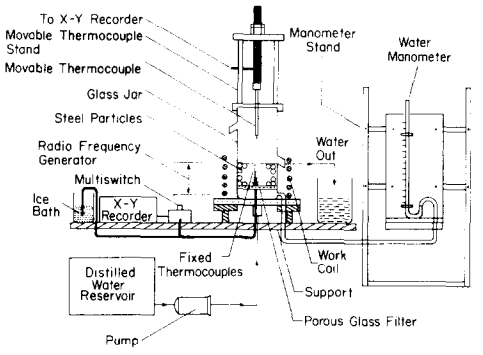

FIG. 2. Schematic diagram of the experimental set-up.

the flat bottom of the quartz jar. The particulate layer is supported on the filter while the space between the filter and the bottom of the jar serves to make the flow uniform at entrance to the porous layer. A 6 mm dia. hole in the filter plate allows insertion of thermocouples from the bottom of the jar. Nine chromel–alumel thermocouples carried in a 0.397 mm dia. two-hole alumina insulators are fixed vertically to the filter so that the hot junctions of the thermocouples are at heights of 3, 13, 25, 38, 50, 63, 75, 88 and 102 mm from the filter. The temperature at other locations in the porous layer can be measured by the movable thermocouple shown in Fig. 3. The thermocouples are connected to a Houston 2000 Omnigraphic $X-Y$ recorder through a multi-switch. After ascertaining that the jar diameter did not have an effect on the pressure drop, experiments for porous layers deeper than 20 cm were conducted in a 51 mm dia. glass jar. This jar was instrumented in the same fashion as the 102 mm dia. jar.

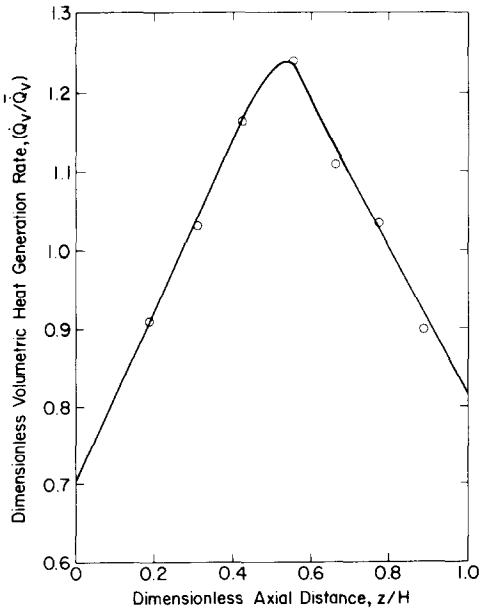

FIG. 3. Typical variation of dimensionless volumetric heat generation rate in the porous layer.

The reservoir containing distilled water at room temperature is connected to the inlet of the quartz jar via a 0.75 HP centrifugal pump and a control valve. The multi-turn work coils are made of either 4.76 mm or 9.5 mm o.d. copper tubing. The pitch and the diameter of the coils are decided from the power requirements and the height of the particulate layer. To achieve a uniform power distribution, a constant clearance between two consecutive turns is maintained by using three work coil holders. The work coil is connected to either a 10 or 25 kW, 450 kHz cycle-dyne radio frequency generator.

Since the flow velocities studied in this work are small, a natural gravitational separation of steam and water droplets is attained at exit of the two phase mixture from the particulate layer. A calibrated glass jar and a stop watch are used to measure the flow rate of the water at outlet from the particulate layer.

Prior to each experiment, the porosity of the particulate layer was determined by knowing the amount of distilled water needed to saturate the particulate layer of given height. Knowing the jar diameter, the layer height and the volume of water needed to saturate the layer, the porosity of the particulate bed was calculated. Maximum uncertainty in porosity is expected to be less than $\pm 2.5\%$. Calibration for heat generation rate at discrete locations in the particulate layer was made for each particle size, bed height and power setting of the induction heater. The procedure consisted of centering the test cell containing liquid saturated particulate layer in the work coil, switching on the power to the coil and recording the rate of temperature rise at different locations in the particulate layer. Using a lumped capacity method, the local heat generation rate in the particulate layer was determined as

$$\dot{Q}_v = (m_p c_{pp} + m_l c_{pl}) \frac{dT}{dt} / \Delta V \qquad (36)$$

where ΔV was the differential volume of the porous layer of height ΔH. The rate of heat generation generally varied in the axial direction being maximum in the middle and lowest at the top and bottom. A typical distribution of the volumetric heat generation rate in the vertical direction is plotted in Fig. 3. While plotting, the heat generation rate has been non-dimensionalized with the vertically averaged heat generation rate. Maximum uncertainty in the (local) heat generation rate is expected to be less than $\pm 3.5\%$. The heat generation profile such as shown in Fig. 3 was used to set the constants A and B in the expression for the heat generation rate for the regions above and below the plane of maximum heat generation rate.

After calibrating the heat generation rate, the power was switched off and water was allowed to flow through the porous layer until the particles, the liquid and the environment reached thermal equilibrium. The water flow rate was then stopped. The zero reading of the manometer was adjusted with water filling the porous layer. Thereafter the flow rate was

adjusted to a desired value and single phase pressure drop through the porous layer was measured. This observed pressure drop was found to compare quite well with that obtained by using Kozeny–Carman relation (4). The power to the work coil was switched on and the system was again allowed to reach a steady state. The temperatures at various locations in the particulate layer were measured. The flow rate of liquid separated at exit was determined and was used to evaluate the quality, x_e, as

$$x_e = 1 - (\dot{m}_{le}/\dot{m}_l). \quad (37)$$

The manometer reading was noted for the pressure drop across the porous layer. The above procedure was repeated for different exit qualities by varying the inlet flow rate while keeping the total input power constant.

In a few experiments in which vapor channels were observed to form, photographs of the top of the porous layer were also taken.

Data reduction

The temperatures at different locations in the porous layer were evaluated from their traces on the recorder. The temperatures in the single as well as the two phase region were observed to fluctuate a few degrees about the mean value. However, uncertainty in obtaining these temperatures should be less than $\pm 0.5°C$. The sum of friction, acceleration and hydrostatic pressure drops in the boiling region was determined by subtracting from the observed pressure drop, the calculated single phase pressure drop in the non-boiling region. Although uncertainty in the observed pressure difference in most of the experiments is expected to be less than $\pm 11.5\%$, yet in a few of the experiments in which the observed pressure difference was only a few millimetres, the uncertainty could be as high as $\pm 50\%$. The uncertainty in the total pressure drop is less than ($\pm 11.5\%$) the uncertainty in the observed pressure difference since zero of the manometer accounted for the hydrostatic head of the porous layer saturated with liquid. The error in measuring quality of the mixture at exit is expected to be less than $\pm 7.1\%$. An energy balance based on the observed quality was also made and found to compare within about $\pm 15\%$ of the heat generated in the porous layer. The data about diameter and number of channels were obtained by viewing the photographs in a slide microscope with a magnification of 10–70.

RESULTS AND DISCUSSION

A total of 30 experimental runs were made. The pressure drop across the volumetrically heated porous layer was measured in all of the runs while temperature histories and vapor channel parameters were obtained only in representative experiments. In these experiments, the particle sizes studied were 590–790 μm. The porous layer heights were varied from 9.0 to 81.3 cm. The layer porosity in all of the experiments was about

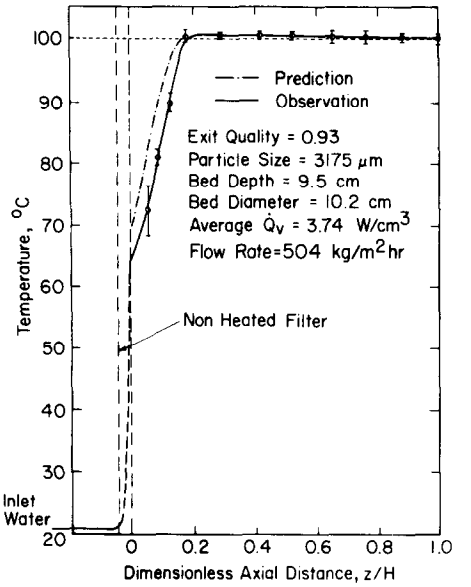

FIG. 4. Comparison of predicted and observed temperature profiles along the direction of flow in the volumetrically heated porous layer.

0.4. The volumetric heat generation rate in the solids was varied between 1.44 and 44.0 W/cm^3 while the flow rate of water was adjusted between 510 and 18200 kg/m^2 h. Complete details of these data are given in [7].

Temperature distribution

A typical temperature distribution obtained in a 10 cm deep porous layer of 3175 μm dia. particles is shown in Fig. 4. In this case water temperature at inlet was 22°C while the flow rate was 0.14 kg/m^{2}s. About 40°C temperature rise is observed to occur in the non-heated filter and is indicative of the axial conduction through the filter. In the single phase region, the temperature of the porous layer and the liquid is observed to increase non-linearly in the vertical direction. When the liquid reaches its saturation tempera-

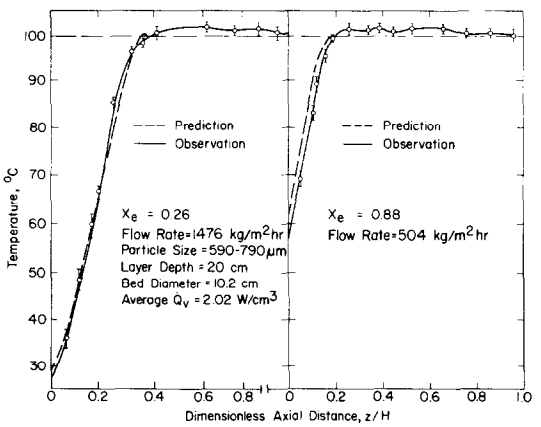

FIG. 5. Comparison of predicted and observed temperature profiles along the direction of flow in the volumetrically heated porous layer.

ture and boiling begins in the particulate layer, the temperature of the porous layer remains nearly constant. In Fig. 4, the temperature distribution obtained by solving the energy equation (12) is also plotted. It is noted that the predicted temperature profile compares quite well with the data. The predicted temperature in the single phase region shows less non-linearity than the observed temperature. The reason for this can be the uncertainty in the local heat generation rates used while integrating the energy equation. The predicted and observed temperature profiles in a 20 cm deep layer composed of 590–700 μm dia. particles are shown in Fig. 5 for exit qualities of 0.26 and 0.88. The agreement between predicted and observed temperatures is again quite good. The observed mean temperatures in the two phase region is a few degrees higher than saturation temperature because of larger superheat experienced by smaller particles.

The temperature data plotted in Figs. 4 and 5 show some variability about a mean value. The higher value probably corresponds to the particle temperature while the lower temperature is that of the fluid. The range of variability in the single phase region is larger than in the two phase region. Figures 3 and 4 also show that the extent of the two phase region increases with increased quality or increased heat generation rate in the particles.

Two phase pressure drop in large diameter particles ($d_p > 1600\,\mu$m). The total two phase pressure drop non-dimensionalized with hydrostatic pressure of saturated water layer of height equal to the boiling region when plotted as a function of exit quality showed [7] that within uncertainty of measurements, the pressure drop was independent of layer height and diameter of the jar. This observation which is valid only as long as the jar diameter is greater than 10 times the particle diameter simplified considerably the correlation of the data with other parameters.

The dimensionless two phase pressure drop is plotted in Fig. 6 as a function of liquid velocity. The data for a given quality can be represented by a single curve drawn through mean of the data. These curves show that for a constant exit quality, the pressure drop decreases with flow velocity (dimensionless pressure drop less than unity) reaches a minimum value and then increases again. The magnitude of the dimensionless pressure at local minima depends both upon the exit quality and the flow velocity. At low flow velocities, the total pressure drop being less than unity implies that reduction in the hydrostatic head due to presence of vapor bubbles in the porous layer overcompensates the friction pressure drop. A positive flow rate through the porous layer can thus be maintained by a liquid column of height equal to the boiling region of the porous layer. At higher flow velocities reduction in the average density of the two phase mixture is unable to keep up with the increased two phase friction drop and the total pressure drop again becomes positive. The data of Fig. 6 also show that for a given pressure drop more energy can be removed at lower flow velocities because the product $G_f x_e$ decreases with increase in flow velocity.

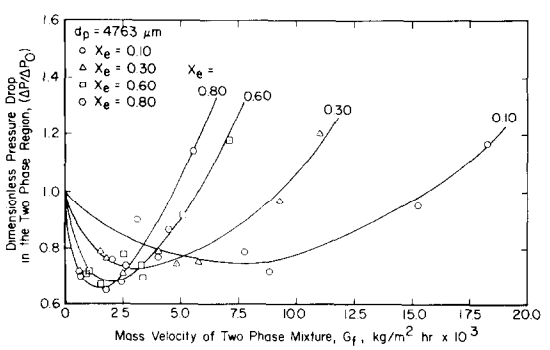

FIG. 6. Dimensionless total pressure drop in porous layer containing 4763 μm dia. particles.

Since the total two phase pressure drop for a given mass flow velocity is observed from Fig. 6 to depend only upon exit quality and the total two phase pressure drop obtained by integrating equation (28) can be based on the average void fraction in the boiling region, the functional dependence of the local void fraction upon the local quality is postulated as

$$\alpha = x^m. \tag{38}$$

The form of equation is also consistent with the requirement that $\alpha = 0$ at $x = 0$ and $\alpha = 1$ at $x = 1$. Using α given by equation (38), equation (28) is integrated to determine for different flow rates and heat generation rates, the total pressure drop in the boiling region of a porous layer. The value of the exponent, m, which results in the calculated pressure drop to be equal to the observed pressure drop is then determined. Figure 7 shows a plot of m as a function of inverse mass velocity for porous layers composed of 3175 and 4763 μm dia. particles. All of the values of m representing all the exit qualities and the porous layer heights studied are correlated within $\pm 50\%$ as

$$m = 0.359 + 626 G_f^{-1}. \tag{39}$$

In equation (39), G_f, is the mass velocity in kg/m^2 h. Figure 8 compares the observed two phase pressure drop with the pressure drop predicted by using the exponent, m, given by equation (39). To test the validity of the predictions, Fig. 8 contains not only the data for 3175 and 4763 μm dia. particles but also the data obtained with 1588 μm dia. particles. The predicted pressure drop for all the 89 data points plotted in Fig. 8 lie within $+38\%$ and -28% of the observed pressure drop. The root mean square deviation of the predicted pressure drop from the observed pressure drop is $\pm 15.1\%$.

Two phase pressure drop in small diameter particles ($d_p < 1600\,\mu$m). Visual observations showed that in porous layers composed of 590–790 μm dia. particles vapor escaped in the form of channels or tunnels located discretely in the porous layer. The vapor channels were free of particles but a few times liquid

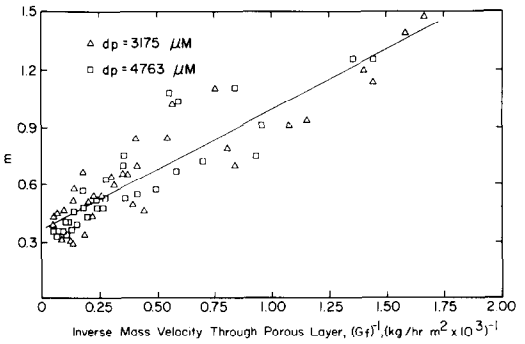

FIG. 7. Correlation of exponent m with inverse mass velocity.

droplets were observed to eject out of these channels. The photograph in Fig. 9 shows a typical top view of the vapor channels at exit of the two phase mixture. Considerable information on the physical parameters pertaining to vapor channels has been generated from photographs such as shown in Fig. 9. The channel diameter at exit has been found to vary between 1.9 and 4.1 mm. The fractional area of the porous layer occupied by vapor channels at exit has been observed to vary between 0.08 and 0.28. For a given quality, the area occupied by the channels is observed to decrease slightly with increase in height of the porous layer and is nearly independent of the exit quality. The vapor channel diameter, d_{ce}, at exit and the number of channels per unit cross-sectional area of the porous layer, N, are correlated with exit quality and height of the two phase region as

$$d_{ce} = 0.26x_e^{0.10}(H - z_l)^{0.07} \quad (40)$$

and

$$N = 4.29x_e^{-0.16}(H - z_l)^{-0.26} \quad (41)$$

In equations (40) and (41), d_{ce} is measured in centimetres.

The two phase pressure drop in porous layers composed of 590–790 μm dia. particles when non-

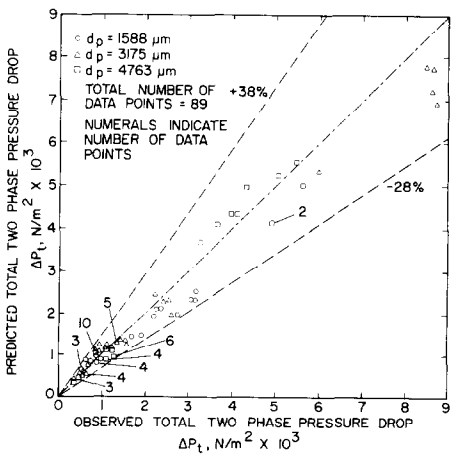

FIG. 8. Comparison of predicted and observed total two phase pressure drop for 1588, 3175 and 4763 μm dia. particles.

FIG. 9. Vapor channels as observed in a porous layer composed of 590–790 μm dia. particles.

dimensionalized with hydrostatic head of saturated water layer of height equal to a boiling region did not show any dependence on the height of the boiling region. This behavior is similar to that observed earlier for large diameter particles. Figure 10 shows a plot of dimensionless two phase pressure drop as a function of the mass velocity, G_f. It is noted that data for a given exit quality can be represented by a single curve. The mean curves drawn through the data show that the dimensionless pressure drop increases nearly as square

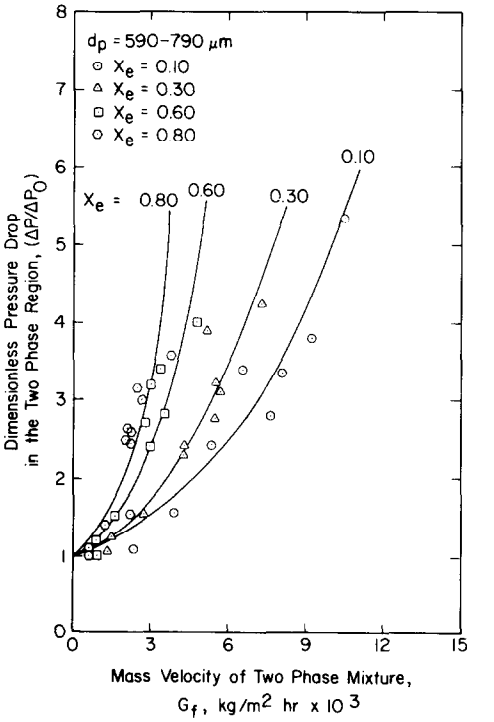

FIG. 10. Dimensionless total pressure drop in a porous layer composed of 590–790 μm dia. particles.

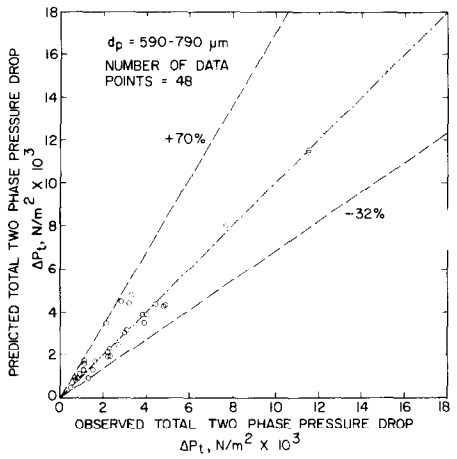

FIG. 11. Comparison of observed total two phase pressure drop with that predicted by the channeled flow model for 590–790 μm dia. particles.

of mass velocity. The data plotted in Fig. 10 can be correlated within $\pm 20\%$ as

$$\frac{\Delta P_t}{\Delta P_0} = 1 + 1.27 \times 10^{-6} x_e^{0.71} G_f^{1.8}$$

$$\text{for } G_f \leq 10^4 \text{ kg/m}^2 \text{ h}. \quad (42)$$

It can be seen from Fig. 10 or the correlation equation (42) that for a given pressure drop the product $x_e G_f$ is higher at lower values of G_f. This suggests that more energy can be dissipated at lower mass velocities since the product $x_e G_f$ is proportional to the energy removed from the porous layer. This observation can be of significant importance in assessing the coolability of a degraded core of a nuclear reactor when the core is assumed to behave as a porous layer of small particles such that vapor channels form in the core.

The total two phase pressure drop predicted by using the model and procedure described for small diameter particles in the section on analysis is plotted in Fig. 11 against the observed pressure drop. The predicted pressure drop is obtained by taking the constant c_0 in equation (31) to be 3200. The predicted pressure drops lie within $+70\%$ and -32% of all the two phase pressure drop data obtained with 590–790 μm dia. particles. Only a few data points at very low flow velocities lend to such a large deviation as the root mean square difference between the predicted and observed pressure drops is $\pm 25.5\%$. For the maximum flow velocity and exit quality studied, the Reynolds number at exit of vapor channels is found to be 1100. This justifies our assumption of laminar flow in the vapor channels.

The total two phase pressure drops predicted by the homogeneous and the channeled flow models are plotted in Fig. 12 as a function of particle diameter. The predictions are made for a 10 cm deep porous layer with a mass velocity of 9800 kg/m² h, exit quality of 0.35 and exit pressure of 1 atm. Water entering the porous layer with a subcooling of about 78°C, reaches the saturation temperature at 2.9 cm from inlet. In this figure the total pressure drop obtained by minimizing the pressure drop with respect to void fraction is also plotted. For particle diameter less than 2000 μm, the pressure drop predicted by channel flow model is less than the homogeneous model. Evidently the smaller pressure drop given by the channel flow model is a result of formation of vapor channels which are free of particles. As the characteristic dimension of the interstitials increases with the particle diameter, the advantage gained by formation of channels diminishes. The channel flow model predicts slightly higher total pressure drop than the homogeneous model for par-

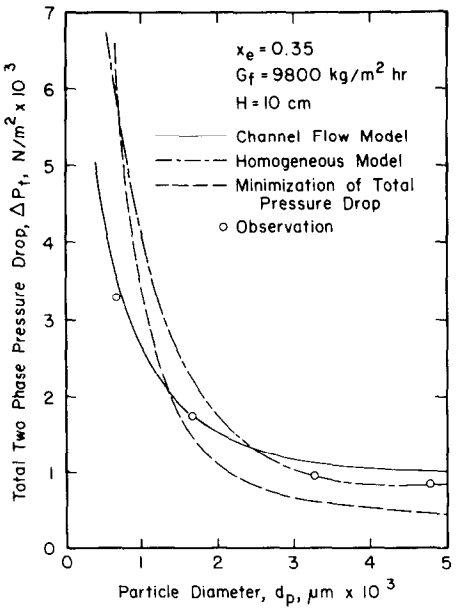

FIG. 12. Comparison of total two phase pressure drop predicted by various models.

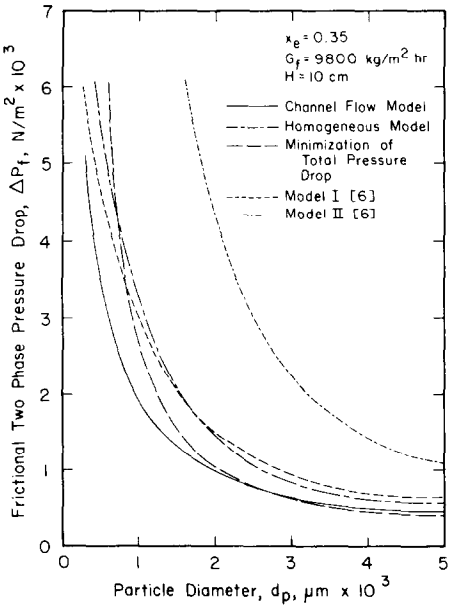

FIG. 13. Comparison of two phase friction pressure drops predicted by various models.

ticle diameters greater that 2500 μm. The total pressure drop based on minimization principle is much less than that given by homogeneous and channel flow model when the particle diameter is greater than 2000 μm. For particles smaller than 1000 μm, the pressure drop based on minimization principle is much higher than that predicted by the channel flow model.

Figure 13 shows the friction pressure drop obtained by subtracting the hydrostatic head from the total pressure drop plotted in Fig. 12. In Fig. 13, the friction pressure drops given by Vasiliev and Maiarov's [6] models I and II are also plotted. For particle diameter greater than 2000 μm, the pressure drop predicted by all the models except Vasiliev's model II fall within 20% of each other. The channel flow model gives the lowest pressure drop for particles smaller than 1000 μm dia. The pressure drop predicted by the other four models are 50–300% higher than that predicted by the channel flow model when the particle diameter is 600 μm. The friction pressure drop given by Vasiliev and Maiarov's model II is several times higher than that predicted by the other four models.

CONCLUSIONS

(1) Data for temperature distribution and pressure drop in volumetrically heated porous layers of 590–790, 1588, 3175 and 4763 μm dia. particles cooled by forced flow evaporation of water have been obtained.

(2) The observed temperature distributions in the single and two phase region are found to compare well with the predictions.

(3) Vapor channels are observed to form in porous layers composed of particles with diameter less than 1600 μm. The total two phase pressure drop in these layers is observed to increase with flow velocity and exit quality.

(4) In porous layers of larger particles (d_p = 3175 and 4763 μm) vapor moves through the interstitial spaces. Depending upon the flow velocity the total pressure drop through the porous layer can be less than or greater than the static head of saturated liquid layer of height equal to the height of the boiling region.

(5) Semi-theoretical models have been developed to describe the two phase pressure drop in small and large diameter particles. The predicted pressure drops compare well with the observed pressure drops.

Acknowledgement—This work received partial support from Electric Power Research Institute under agreement RP 1931-1 with Dr. L. Thompson as project manager.

REFERENCES

1. M. V. Choudhary and N. M. El-Wakil, Heat transfer and flow characteristics in conductive porous media with energy generation, *Proc. Int. Heat Transfer Conf., Versailles, France* (1970).
2. W. W. Marr and R. M. Crawford, Porous heat generating blockage in a fuel assembly, *Trans. Am. Nucl. Soc.* **15,** 350 (1972).
3. D. Moalem and S. Cohen, Theoretical analysis of steady and transient operation of internally energized porous element under phase conversion and vapor superheat, *Int. J. Heat Mass Transfer* **19,** 1415–1423 (1976).
4. D. Moalem and S. Cohen, Non Darcy flow with change of phase in internally energized flat shaped porous element, *Int. J. Heat Mass Transfer* **22,** 1165–1174 (1979).
5. D. Moalem, Steady state heat transfer within porous medium with temperature dependent heat generation, *Int. J. Heat Mass Transfer* **19,** 529–537 (1976).
6. L. L. Vasiliev and V. A. Maiarov, An analytical study of resistance, heat transfer and stability in evaporative cooling of a porous heat producing element, *Int. J. Heat Mass Transfer* **12,** 301–307 (1979).
7. A. S. Naik, Forced flow evaporate cooling of a volumetrically heated porous layer, M.S. Thesis, UCLA (1981).

ECOULEMENT FORCE D'UN REFRIGERANT S'EVAPORANT DANS UNE COUCHE POREUSE CHAUFFEE DANS SON VOLUME

Résumé—On étudie expérimentalement la montée en température et la chute de pression d'un réfrigérant qui s'évapore en passant à travers une couche poreuse chauffée dans son volume. Les données expérimentales sur la distribution de température et sur la chute de pression dans la direction de l'écoulement sont obtenues pour de l'eau s'écoulant à travers des couches de particules d'acier chauffées par induction. Des particules sphériques d'acier variables en taille de 590 μm à 4763 μm sont utilisées pour former des couches poreuses dans des colonnes de verre de 5 à 10 cm de diamètre. Dans ces expériences les mesures sont faites pour des épaisseurs de couche variant entre 9 et 81 cm, des sources volumétriques de chaleur entre 1,44 et 44 W cm^{-3} et des débits massiques d'eau entre 510 et 18200 kg m^{-2} h^{-1}.

Un modèle théorique pour le profil de température dans le domaine liquide diphasique est proposé et il s'accorde bien avec les mesures. Des canaux de vapeur sont observés dans les couches poreuses de particules ayant des diamètres inférieurs à 1600 μm. Des modèles semi-théoriques sont développés pour la chute de pression en diphasique pour les particules plus petites ou plus grandes que 1600 μm.

VERDAMPFUNGSKÜHLUNG EINER VOLUMETRISCH BEHEIZTEN PORÖSEN SCHICHT BEI ERZWUNGENER STRÖMUNG

Zusammenfassung—In dieser Arbeit wird über experimentelle Untersuchungen der Temperaturerhöhung und des Druckabfalls eines verdampfenden Kühlmittels, das durch eine volumetrisch beheizte poröse Schicht strömt, berichtet. Temperaturverteilung und Zweiphasen-Druckabfall in Strömungsrichtung wurden für Wasser, das durch induktiv beheizte Stahlpartikel-Schichten strömt, experimentell ermittelt. Die porösen Schichten wurden aus Stahlkugeln der Größe 590 bis 4763 μm in Glaskolben mit 5 und 10 cm Durchmesser gebildet. Die Tiefe der Schichten war 9 bis 81 cm, die volumetrische Heizleistung 1,44 bis 44,0 W/cm^3 und die Massenstromdichte des Wassers 510 bis 18,200 kg/m^2 h.

Für das Temperaturprofil im Flüssigkeits- und im Zweiphasengebiet wurde ein theoretisches Modell erstellt und in guter Übereinstimmung mit den Messungen befunden. In porösen Schichten mit Partikel-Durchmessern unter 1600 μm wurde die Bildung von Dampfkanälen beobachtet. Für den Zweiphasen-Druckabfall bei Partikeln mit Durchmessern, die kleiner und größer als 1600 μm waren, wurden getrennte halb-theoretische Modelle entwickelt.

ПРИНУДИТЕЛЬНОЕ ИСПАРИТЕЛЬНОЕ ОХЛАЖДЕНИЕ ОБЪЕМНО НАГРЕВАЕМОГО ПОРИСТОГО СЛОЯ

Аннотация — Проведено экспериментальное исследование роста температуры и перепада давления при течении испаряющегося теплоносителя в объемно нагреваемом пористом слое. Экспериментальные данные по распределению температур и перепаду давления в двухфазном потоке по направлению течения получены для случая воды, текущей через слои индуктивно нагреваемых стальных частиц. В качестве материала для пористых слоев использовались сферические стальные частицы размером от 590 мкм до 4763 мкм, которые помещались в стеклянные сосуды диаметром 5 и 10 см. Исследовались слои глубиной от 9 до 81 см. Плотность тепловыделения изменялась от 1,44 до 44,0 Вт/см^3, а массовая скорость течения — в диапазоне 510–18200 кг/м^2 ч.

Предложена теоретическая модель для определения профиля температур в жидкости и двухфазной области и найдено, что она хорошо согласуется с результатами измерений. Найдено, что в пористых слоях частиц диаметром менее 1600 мкм образуются паровые каналы. Представлены также полуэмпирические модели для расчета перепада давления в двухфазном потоке для частиц диаметром меньше и больше 1600 мкм.